PHYSICAL REVIEW C **90**, 011302(R) (2014)

Isobaric analog resonances of ^{31}Mg and the border of the island of inversion

N. Imai,[1,*] M. Mukai,[2] J. Cederkäll,[3] H. Aghai,[4] P. Golubev,[3] H. T. Johansson,[5] D. Kahl,[6] J. Kurcewics,[4] T. Teranishi,[7] and Y. X. Watanabe[1]

[1]*Institute of Particle and Nuclear Studies, High Energy Accelerator Research Organization (KEK), Oho 1-1, Tsukuba, Ibaraki 305-0801, Japan*

[2]*Institute of Physics, University of Tsukuba, Tennodai 1-1-1, Tsukuba, Ibaraki 305-8571, Japan*

[3]*Department of Physics, Lund University, Box 118, SE-221 00 Lund, Sweden*

[4]*PH-Department, CERN, CH-1211 Geneva 23, Switzerland*

[5]*Department of Fundamental Physics, Chalmers University of Technology, SE-412 96 Göteborg, Sweden*

[6]*Center for Nuclear Study, The University of Tokyo, RIKEN Campus, 2-1 Hirosawa, Wako, Saitama 351-0198, Japan*

[7]*Department of Physics, Kyushu University, 6-10-1 Hakozaki, Fukuoka 812-8581, Japan*

(Received 19 June 2013; revised manuscript received 10 June 2014; published 15 July 2014)

The evolution of the nuclear shell structure in the region of the neutron-rich shell-breaking nucleus ^{32}Mg has been the subject of considerable interest. We present here the first determination of the overlap of the ground and two first excited states in ^{31}Mg with a neutron coupled to the ground state in ^{30}Mg based on studies of its isobaric analog resonances in ^{31}Al. The excitation function for proton resonant elastic scattering on ^{30}Mg was measured close to 0° in the laboratory frame by bombarding a thick polyethylene target with a ^{30}Mg beam at an energy of 2.92 MeV/nucleon at the REX-ISOLDE facility at CERN. Three resonances were successfully resolved, and angular momenta and total and proton resonance widths were determined by using R-matrix analysis. The deduced spectroscopic factor for the ground state in ^{31}Mg is consistent with the shell-model calculation, whereas those for the first and second excited states could not be reproduced. These results show that a drastic change in structure occurs between ^{30}Mg and ^{31}Mg and that the onset of structural change in this region therefore occurs between these two isotopes.

DOI: 10.1103/PhysRevC.90.011302 PACS number(s): 23.20.Js, 21.10.Tg, 27.30.+t, 29.30.Kv

The conjecture that nuclear shell closures persist over large ranges of neutron and proton numbers was central for the development of nuclear theory, and it has remained a linchpin for nuclear modeling ever since the pioneering work of Mayer and co-workers [1]. However, it has also been speculated in recent years that the energy of nuclear orbits may shift significantly with the neutron-to-proton ratio so that well-known shell closures vanish and new ones appear far from stability. Drivers for such structure changes may include the underlying nucleon-nucleon interaction [2]. An unexpected first indication that major changes in nuclear shell structure can occur far from stability came with the observation of large two-neutron separation energies in ^{31,32}Na by Thibault *et al.* [3]. Much experimental effort has since then gone into pinning down the causes of this phenomenon [4,5], but so far, no measurement of wave-function overlaps has been performed to identify the point where the ν(2p-2h) configuration rather than the ν(0p-0h) configuration is dominant in the ground state (g.s.). The idea behind the current experiment is therefore to investigate wave-function differences between ^{31}Mg and a neutron coupled to the ground state of ^{30}Mg.

The experiments have also been accompanied by new theoretical work. Calculations that use an expanded model space discussed in Ref. [6] led to the notion that the observed effect is a consequence of neutron excitations from the *sd* shell into the *pf* shell across the magic number $N = 20$. The calculations also predicted that an "island of inversion" for $10 \leqslant Z \leqslant 12$ and $20 \leqslant N \leqslant 22$ should exist where the ground-state configuration is dominated by intruder ν(np-nh) configurations. Indeed, the masses of ^{30,31}Mg were well reproduced by the normal ν(0p-0h) configuration [7], which suggests that these nuclei do not belong to the island of inversion. However, the most recent experiments aimed at mapping the border of the island of inversion reveal that the region is wider than expected [8–10].

^{31}Mg has been extensively studied in the past since it has been considered to be located at the edge of the island of inversion [11]. A g-factor measurement of the ground state in ^{31}Mg determined the spin and parity (J^π) as $1/2^+$ [12] instead of the $3/2^+$ expected for a spherical nucleus with $N = 19$. In the framework of the Nilsson model, this J^π can be explained with a large deformation of $\beta \sim 0.4$ [11,12]. This observation is also well reproduced by a calculation in the framework of the antisymmetrized molecular dynamics (AMD) plus generator coordinate model (GCM) [13]. In recent shell-model (SM) calculations, the same phenomenon has been explained by introducing an enhanced tensor force [14]. On the other hand, ^{30}Mg can be considered to be situated outside the island of inversion, although the deformation parameter $\beta = 0.41$ for ^{30}Mg deduced from the reduced transition probability $B(E2; 0^+_{\text{g.s.}} \rightarrow 2^+_1) = 241(31)\ e^2\ \text{fm}^4$ [15] is as large as that of ^{31}Mg. Indeed, the second 0^+ state was populated in ^{32}Mg in a two-neutron transfer reaction on ^{30}Mg [16]. The transition from this state to the ground state of ^{32}Mg, which is considered to consist mainly of the ν(2p-2h) configuration, was found to be hindered. This suggests that the ground state of ^{30}Mg is dominated by the ν(0p-0h) configuration. To compare the

*nobuaki.imai@kek.jp

populations of the negative-parity states after neutron knockout from ^{30,32}Mg also suggests that ^{30}Mg is outside the island of inversion [17]. These studies together suggest that the limit of the island of inversion is located at ^{30,31}Mg. However, neither direct evidence nor the degree of structural change can be obtained from studies of the kind mentioned. Moreover, the reanalysis of the two-neutron transfer reaction suggests that the ground state in ^{32}Mg is normal ν(0p-0h) [18]. As such, the overlap of the wave functions for ^{30,31}Mg needs to be measured.

In contrast to the ground state of ^{31}Mg, the J^π's of the other bound states have been assigned based on the multipolarities of the γ transitions as estimated from their lifetimes. The J^π's for the first and second excited states were assigned to be $3/2^+$ and $3/2^-$, respectively [19,20].

In this Rapid Communication, we investigate the three lowest-lying bound states in ^{31}Mg through their isobaric analog resonances (IARs) which appear at high excitation energies in ^{31}Al. When the analog state is above the proton separation energy (S_p), it is observed in the excitation function of proton elastic scattering on ^{30}Mg as an IAR. The resonance energy (E_R), spectroscopic factor (S^{pp}), and angular momentum (l) can be deduced by R-matrix analysis [21,22] of the excitation function at a given scattering angle. Proton resonant elastic scattering can be measured in inverse kinematics with a low-energy radioactive ^{30}Mg beam and a thick proton target. We have recently applied this method to the unstable nucleus ^{35}Si and successfully have derived the spectroscopic information as discussed in Ref. [23].

The energy difference between the ground states of ^{31}Mg and ^{31}Al is 11 833(40) keV [24]. The energy difference between the IAR and the corresponding parent state is determined by the Coulomb displacement energy (Δ_c) and the proton-neutron mass difference (δ_{pn}). By using an empirical formula for Δ_c [25], each IAR is expected to be located above the parent state by 3978 keV. Since the S_p of ^{31}Al is 13 360(14) keV, one expects to observe IARs in the excitation function for proton elastic scattering at a center-of-mass energy ($E_{\mathrm{c.m.}}$) above 2451 keV.

The experiment was performed at the ISOLDE facility at CERN [26]. The radioactive atoms of ^{30}Mg were produced by impinging 1.4-GeV protons, provided by the CERN PS Booster with a maximum intensity of 3×10^{13} protons/pulse and a repetition time of typically 1.2 s, on a uranium carbide target. The Mg atoms which diffused out of the target were selectively ionized in the resonance ionization laser ion source [27] where three-step lasers were directed. The Mg^+ ions masses analyzed by the ISOLDE High Resolution Separator were charge bred to Mg^{7+}, then were accelerated up to 2.92 MeV/nucleon with the REX-ISOLDE postaccelerators [28]. The 1×10^5 particles/s beams were directed onto a secondary target of 5.6-mg/cm^2-thick polyethylene where they were stopped. A 10.9-mg/cm^2-thick carbon target was also used to determine effects from carbon-induced reactions in the polyethylene. The ions were delivered through two apertures; one had a 5-mm diameter and was located 1.5 m upstream of the target, whereas the other was 10 mm in diameter located just upstream of the target. These two apertures restricted the incident angles to less than 0.28°.

Two layers of silicon semiconductor detectors were placed at 0° to measure the outgoing particles. They were 115 mm downstream of the target. The respective thicknesses were 0.31 and 1.0 mm. The detectors' active areas were 58×58 mm^2. The first layer was double sided and with orthogonally oriented $32 + 32$ strips, which allowed us to determine the scattering angles of the outgoing particles.

The $E_{\mathrm{c.m.}}$ was deduced from the measured proton energy and the scattering angle on an event-by-event basis by assuming elastic-scattering kinematics and by considering the energy losses of the beam ions and the protons in the target. The energy losses were estimated by using the SRIM-2011 code [29]. The energy resolution in the laboratory frame was estimated to be 80 keV (1σ), which arose mainly from the energy spread due to the uncertainty of the scattering angle of 0.8°. The particles detected were identified by the ΔE-E method. The total energy deposited in the detectors was calibrated by measuring the proton resonant elastic scattering on ^{26}Mg by using a 2.86-MeV/nucleon ^{26}Mg beam, whose excitation function had been measured precisely [30]. The measured proton energies were calibrated to reproduce the strong resonance at $E_{\mathrm{c.m.}} = 2049$ keV. The energies were determined to within 10 keV in $E_{\mathrm{c.m.}}$.

No detector was placed in the beamline to determine the number of incident-beam ions since that would have reduced the beam energy and consequently the scanning range for the excitation function. The protons induced by background ions can be evaluated by turning off the first-step laser. The background ions were the surface-ionized ^{30}Al and unknown ions from the residual gas of the charge breeder. The relative normalization factor of the spectrum without the laser to the one with the laser was determined by comparing the number of detected protons which were produced between 200 and 600 ms after the proton synchrotron impact when the ^{30}Mg beam was not extracted. As illustrated in Fig. 1, protons related to the resonances appear within 100 ms of the impact. The normalized spectrum measured with the laser off was subtracted from that measured with the laser on. Then, the target thickness for each 20-keV loss of the beam in the c.m. at the respective energy was taken into account in

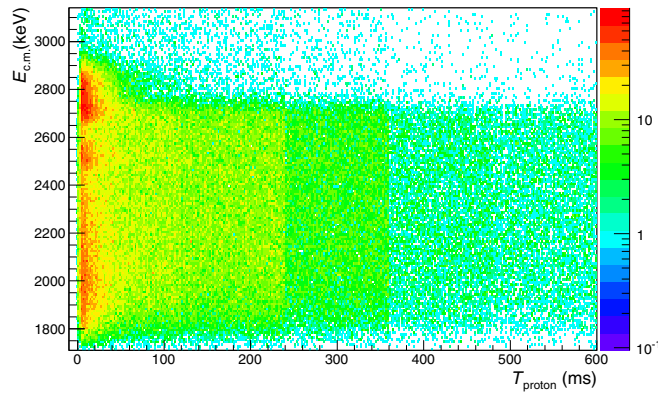

FIG. 1. (Color online) Correlation between $E_{\mathrm{c.m.}}$ and the detection time (T_{proton}) after each proton synchrotron impact. Resonance loci can be seen within 100 ms after the impact.

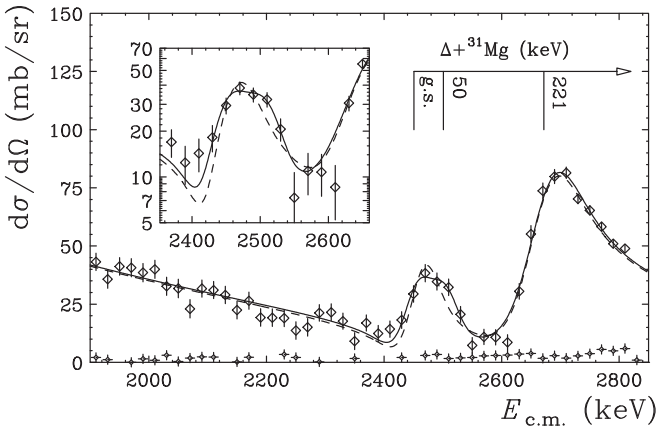

FIG. 2. Excitation functions of the proton elastic scattering. Cross sections measured with the polyethylene target (diamonds) and the carbon target (crosses). The solid (dashed) line denotes the best-fit R-matrix calculation by assuming three (two) resonances. The region of $E_{\mathrm{c.m.}} = 2350$–2660 keV is illustrated in the inset. The expected resonance energies are also presented. The IARs would appear higher than 2400 keV. See text for details.

determining the cross section. The absolute cross section was obtained by normalizing the off-resonant cross sections of the proton elastic scattering on ^{30}Mg for $E_{\mathrm{c.m.}} \leqslant 2400$ keV where there is no IAR. Two significant resonances were clearly observed in the excitation function as presented in Fig. 2. The expected energies of the resonances are also presented. Here, $\Delta \equiv \Delta_c + \delta_{pn} - S_p$. The error was derived from the statistical uncertainties only.

The excitation function measured with the carbon target is also shown in Fig. 2. The relative normalization of the cross sections to those measured with the polyethylene target was deduced by comparing the number of protons for $E_{\mathrm{c.m.}} > 2830$ keV that cannot be produced by elastic scattering. The carbon contribution was found to be negligibly small.

The shape of each resonance and the interference between resonances are determined by their orbital angular momenta. R-matrix calculations were performed to determine l, the resonance parameters E_R, proton width (Γ_p), and total width (Γ_{total}). By assuming the l values for each resonance, a minimum value of χ^2 (χ^2_{min}) was searched for by changing the normalization of the cross sections and the resonance parameters by using MINUIT [31]. The R-matrix curve was obtained as the sum of the single resonances and was folded with the experimental resolution of 20 keV in the c.m. frame. In the calculation, the potential scattering was obtained by using the global optical-model potential set [32].

First, we tried to fit the calculation to the experimental data by assuming each l with seven free parameters for two resonances, namely, two Γ_p's, two Γ_{total}'s, two E_R's, and the absolute normalization. The initial E_R's were 2480 and 2640 keV, respectively, estimated from the peak energies. The best $\chi^2_{\mathrm{min}} = 65.5$ with 43 degrees of freedom was obtained for the combination of $l = 0$ and 1. The obtained resonance parameters that assume the respective angular momenta are listed in Table I. When we assumed $l = 2,1$, the $\chi^2_{\mathrm{min}} = 88.8$ was presented for parameter set 2. When we assumed $l = 3$ for the second resonance, which is most likely for the lowest negative-parity state of an $N = 19$ nucleus, the dip between the two resonances was not reproduced. The obtained χ^2_{min}'s were much larger than those that assumed the second resonance of $l = 1$ as shown by parameter sets 3 and 4, which ruled out an $l = 3$ assignment for the second resonance. When we assumed both resonances were positive-parity states, the $\chi^2_{\mathrm{min}} = 92.9,690$ for $l = (2,0),(0,2)$ was shown by parameter sets 5 and 6, respectively. The negative-parity assignment for the first resonance, which is unlikely for the ground state of an $N = 19$ nucleus, was also rejected by the fitting as displayed for parameter set 7.

Even with parameter set 1, the resultant R-matrix calculation demonstrated by the dashed line in the inset of Fig. 2 still failed to reproduce the first peak around $E_{\mathrm{c.m.}} = 2460$ keV, which suggests that another resonance should be included. We therefore searched for χ^2_{min} with ten free parameters: three Γ_p's, three Γ_{total}'s, three E_R's, and the absolute normalization by adding a $J^\pi = 7/2^-$ resonance at 2450 keV. The obtained parameters are tabulated as parameter set 8. Here, $\chi^2_{\mathrm{min}} = 55.6$ with 40 degrees of freedom was obtained. On the other hand, when we added a $3/2^+$ state instead of a $7/2^-$ one, $\chi^2_{\mathrm{min}} = 54.5$ was obtained, which clearly supports this assignment. The result, the resonance parameters of which are listed as parameter set 9 in Table I, is presented by the solid line in

TABLE I. Resonance parameters obtained by the R-matrix analysis that assumes two or three resonances. The assumed angular momenta are listed in the second column. The χ^2_{min} obtained with each set is shown in the third column where ndf is the number of degrees of freedom. The superscripts for each resonance parameter from the fourth to the ninth columns denote the order of the resonance from the lowest energy. All the resonance parameters are given in keV. Only the statistical uncertainty is presented. See text for details.

Set	l_i	χ^2_{min}/ndf	$E_R^{(1)}$	$\Gamma_p^{(1)}$	$\Gamma_{\mathrm{total}}^{(1)}$	$E_R^{(2)}$	$\Gamma_p^{(2)}$	$\Gamma_{\mathrm{total}}^{(2)}$	$E_R^{(3)}$	$\Gamma_p^{(3)}$	$\Gamma_{\mathrm{total}}^{(3)}$
1	0,1	65.5/43	2459(3)	17(2)	17 (6)	2666(4)	76(3)	104(2)			
2	2,1	88.8/43	2492(3)	3.4(3)	3.4(24)	2673(2)	87(3)	119(2)			
3	2,3	284/43	2571(4)	81(4)	161(3)	2684(2)	79.9(3)	159(1)			
4	0,3	999/43	2465(4)	12(2)	12 (2)	2698(1)	40.0(9)	80.0(3)			
5	2,0	92.9/43	2500(6)	5.4(6)	5.4(6)	2676(2)	90(3)	121(3)			
6	0,2	690/43	2449(6)	3.7(12)	5.5(18)	2778(2)	105(6)	131(3)			
7	1,0	88.8/43	2447(4)	41(7)	83.6(5)	2657(4)	64(2)	92(2)			
8	0,3,1	55.6/40	2445(12)	10(5)	10 (9)	2493(1)	0.7(9)	0.7(2)	2668(3)	79(4)	109(2)
9	0,2,1	54.5/40	2446(4)	13(5)	15 (8)	2509(2)	1.3(5)	1.3(13)	2668(3)	79(4)	109(2)

Fig. 2, which demonstrates good agreement with the data. The almost identical values of Γ_p and $\Gamma_{\rm total}$ suggest that they are IARs of the bound states in ^{31}Mg because, for the lower-isospin excitation, the neutron channel should be open so that $\Gamma_p < \Gamma_{\rm total}$.

The obtained E_R of the first resonance is close to the expected value of 2451 keV, which supports the notion that the first resonance is the IAR of the ground state of ^{31}Mg. $E_{\rm ex}^{pp}$ in the third column in Table II represents the energy difference with respect to the lowest resonance. The $E_{\rm ex}^{pp} = 63(4)$ and 222(5) keV show good consistency with the excitation energies of 51 and 221 keV for the first two excited states in ^{31}Mg, which supports the identification of the IARs.

The present assignment of $J^\pi = 1/2^+$ for the first resonance is also in agreement with the g-factor measurement of ^{31}Mg. The l values determined for the second and third resonances confirm the assignments of $J^\pi = 3/2^+$ and $3/2^-$ for the first and second excited states in ^{31}Mg. Hereafter, we adopt these J^π's for both bound excited states.

The S^{pp} can be deduced from Γ_p by using the formula [22],

$$S^{pp} = \left[\frac{(N-Z+1)2\mu r \Gamma_p}{2P_c^0 e^{-2\delta^{I_{lj}}} \hbar^2 u_n^2(r)} \right]_{r=a_c}, \qquad (1)$$

where N is the number of neutrons in the target nucleus, μ is the reduced mass of the proton-^{30}Mg system, P_c^0 is the optical penetrability, $a_c = 1.40 \times (\sqrt[3]{30} + 1) = 5.8$ fm is used as the matching radius, and $u_n(r)$ is the single-particle wave function of a bound-state neutron in the parent state of (l, j). a_c was selected as the minimum S^{pp} for the respective states.

$\delta^{I_{lj}}$ represents the imaginary part of the optical phase shift, which was obtained by the distorted-wave Born approximation code DWUCK4 [33] with the optical-model potential set of Ref. [32]. The neutron wave function $u_n(r)$ was obtained by solving the Schrödinger equation to reproduce the neutron binding energy of the parent state.

As shown in Fig. 3, the dependence of the matching radius for the S^{pp}'s are rather flat around $a_c = 5.8$ fm, which indicates that the independence of the boundary radius is satisfied [22]. The obtained S^{pp}'s as well as all the parameters employed to deduce them are tabulated in Table II.

For the systematic errors of S^{pp}, it is difficult to estimate them from the current experiment alone. We adopted the deviation between S^{pp} for the IAR of ^{27}Mg and S^{dp} measured by the (d, p) reaction as the systematic error. The S^{pp}'s determined by measuring the IARs of ^{27}Mg were identical with those measured with the (d, p) reaction within 30% [30]

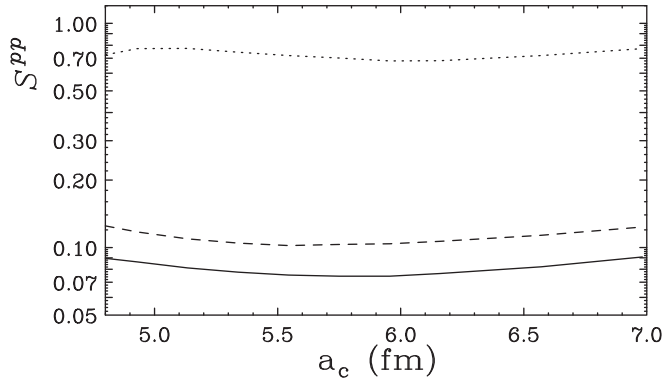

FIG. 3. Dependence of the matching radius for the spectroscopic factors of the three resonances. Solid, dashed, and dotted lines indicate the S^{pp}'s for $1/2^+$, $3/2^+$, and $3/2^-$ resonances, respectively.

in the case of the strong analogs, whose strength is larger than 0.1 in terms of the spectroscopic factor. However, for the weak analog, whose spectroscopic factor is less than 0.1, the S^{pp} of the IAR was observed to be two times larger, which was caused mainly by the lower-isospin excitation. We adopted these differences as the systematic errors in the present Rapid Communication. Namely, for the first and second resonances, the systematic error was estimated as 100%, whereas for the third state, it was 30%. It should be noted that the shape of our R-matrix fit for the third resonance might be affected by higher-energy resonances which are above the $E_{\rm c.m.}$ scanned in the present experiment, and thus we could not include them in the fit.

Spectroscopic factors (S^{dp}), which were measured with the (d, p) reaction [34,35] for the bound low-lying states in $N = 19$ nuclei, are compared with the present results in Fig. 4. For the positive-parity resonances $1/2^+$ and $3/2^+$, the S^{pp}'s for the IARs of ^{31}Mg are determined to be 0.07(3)(7) and 0.10(4)(10), respectively (Table II). On the other hand, for the isotopes ^{37}Ar and ^{35}S, the lowest $3/2^+$ state has $S^{dp} \simeq 0.5$, whereas the first $1/2^+$ state has $S^{dp} \simeq 0.2$. If the lower-isospin excitation made the S^{pp} larger, like the IARs of ^{27}Mg, the spectroscopic factors of these two parent states in ^{31}Mg would be even smaller. The present quenched S^{pp} for the first two resonances in ^{31}Al means that the overlap between the wave function of the valence neutron coupled to the ^{30}Mg core and that of the states in ^{31}Mg is small. This demonstrates directly that the nuclear structure changes between ^{30}Mg and ^{31}Mg. On the other hand, $S^{pp} = 0.68(4)(20)$ for the $3/2^-$ state in ^{31}Mg is

TABLE II. Resultant parameters l, E_R, and Γ_p were obtained by R-matrix analysis. $E_{\rm ex}^{pp}$ is the energy difference of the second or third resonance from the first one. P_c^0, $\delta^{I_{lj}}$, and $u_n(r)$ are the optical penetrability, the imaginary part of the optical phase shift, and the radial neutron wave function of the corresponding parent state. P_c^0 and $u_n(r)$ were calculated with $r = 5.8$ fm. S^{pp} denotes the experimental spectroscopic factors, whereas $S_{\rm AMD}$ and $S_{\rm SM}$ are the theoretical values. The errors of E_R and $E_{\rm ex}^{pp}$ are only statistical, whereas those for S^{pp} correspond to the statistical and systematic uncertainties, respectively.

l	E_R (keV)	$E_{\rm ex}^{pp}$ (keV)	Γ_p (keV)	P_c^0	$e^{-2\delta^{I_{lj}}}$	$u_n(r)$	S^{pp}	$S_{\rm AMD}$	$S_{\rm SM}$
0	2446(4)	0.0	13(5)	1.14	0.75	−0.39	0.07(3)(7)	0.02	0.066
2	2509(2)	63(4)	1.3(5)	0.18	1.03	0.26	0.10(4)(10)	0.04	0.238
1	2668(3)	222(5)	79(4)	0.655	0.77	−0.41	0.68(4)(20)	0.29	0.399

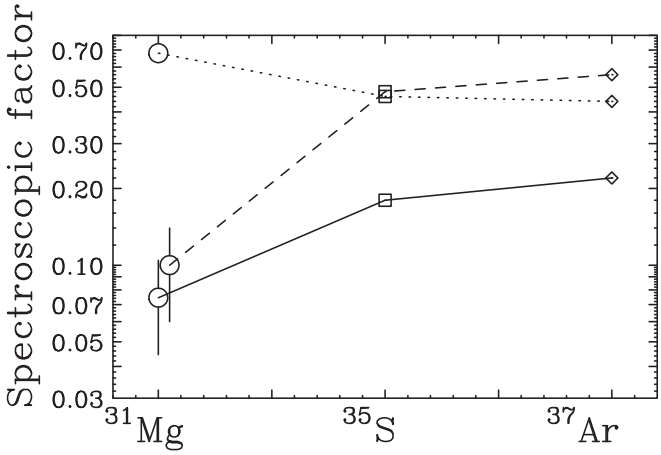

FIG. 4. Spectroscopic factors of the low-lying states in $N = 19$ isotopes. Solid, dashed, and dotted lines stand for the lowest $1/2^+$, $3/2^+$, and $3/2^-$, respectively. The spectroscopic factors of the corresponding states in ^{35}S [35] and ^{37}Ar [34] were determined by (d,p) reactions. Here, only the statistical error is presented, whereas we estimated the systematic error as 100% for the $1/2^+$ and $3/2^+$ states and 30% for the $3/2^-$ state.

more consistent with $S^{dp} = 0.46$ and $S^{dp} = 0.44$ for ^{35}S and ^{37}Ar, respectively. The larger S^{pp} for this parent state in ^{31}Mg indicates that the configuration of the core nucleus of this state does not change in contrast to the low-lying positive-parity states. This result supports the picture of the AMD + GCM calculation where the low-lying negative-parity states mainly have the 1p-2h configuration [13].

Theoretical spectroscopic factors in the framework of the AMD + GCM [36] (S_{AMD}) and the Monte Carlo shell model (S_{SM}) [37] are compared with the present results in Table II. Although all the values of the bound states with the AMD + GCM are almost half of the present ones, the trend in the spectroscopic factors is reproduced. When one takes into account that the deformation parameter of ^{30}Mg is as large as that of the ground state of ^{31}Mg, the suppression of S^{pp} for the positive-parity states is intriguing. In the AMD + GCM calculation, ^{30}Mg is considered to be triaxially deformed with $\beta = 0.3$ and $\gamma = 20^\circ$, which indicates that the nucleus is more softly deformed contrary to the large prolate deformation of ^{32}Mg [36].

In the case of the Monte Carlo shell model where the interaction which reproduces the g factor of ^{31}Mg in Ref. [12] was used, the spectroscopic factor of the ground state is in good agreement with the current value. On the other hand, spectroscopic factors for the first and second excited states fail to be reproduced by the Monte Carlo shell model. The quenched spectroscopic factor for the second exited state might be attributed to an overly large contribution from the ν(2p-2h) configuration in the ground state of ^{30}Mg. The almost pure single-particle structure of the third resonance also suggests that the ground state of ^{30}Mg may be more spherical. It should be noted that, when the USDA interaction in the sd-shell-model space [38] was employed, the spectroscopic factor calculated with the code NUSHELLX [39] is 0.034 for the first $1/2^+$ state, which is also consistent with the present result. The quenched spectroscopic factor for the first resonance may arise partly from its hole-state structure.

To summarize, we have observed three resonances at high excitation energy in ^{31}Al by proton resonance elastic scattering of ^{30}Mg at 2.92 MeV/nucleon in inverse kinematics. By assuming the isospin symmetry of the nuclear force, the present Rapid Communication confirms $l = 2$ and 1 assignments, respectively, for the first and second excited states in ^{31}Mg. The spectroscopic factor deduced from the proton width of the $3/2^-$ resonance is reasonably large, which indicates that the parent state in ^{31}Mg should have the same configuration as ^{30}Mg. On the other hand, the quenched values for the positive-parity resonances are evidence of a drastic change in shell structure between ^{30}Mg and ^{31}Mg. This is the first direct measurement of the boundary of the island of inversion.

We acknowledge the work of the entire ISOLDE staff for their excellent cooperation during the experiment. One of the authors (N.I.) wants to express his deep gratitude for the hospitality extended to him during his stay at ISOLDE. The present work was supported by a Grant-in-Aid for Scientific Research (Grants No. 20244036 and No. 23740215) by the Japan Society Promotion of Science as well as by grants from the Swedish Research Council and the Royal Physiographical Society in Lund.

[1] M. G. Mayer, Phys. Rev. **75**, 1969 (1949); O. Haxel, J. H. D. Jensen, and H. E. Suess, *ibid.* **75**, 1766 (1949).
[2] O. Sorlin and M.-G. Porquet, Prog. Part. Nucl. Phys. **61**, 602 (2008).
[3] C. Thibault, R. Klapisch, C. Rigaud, A. M. Poskanzer, R. Prieels, L. Lessard, and W. Reisdorf, Phys. Rev. C **12**, 644 (1975).
[4] H. Scheit, J. Phys.: Conf. Ser. **312**, 092010 (2011).
[5] K. Heyde and J. L. Wood, Rev. Mod. Phys. **83**, 1467 (2011).
[6] E. K. Warburton, J. A. Becker, and B. A. Brown, Phys. Rev. C **41**, 1147 (1990).
[7] N. A. Orr *et al.*, Phys. Lett. B **258**, 29 (1991).
[8] A. Gade and T. Glasmacher, Prog. Part. Nucl. Phys. **60**, 161 (2008), and references therein.
[9] P. Doornenbal *et al.*, Phys. Rev. Lett. **103**, 032501 (2009).
[10] G. Christian *et al.*, Phys. Rev. Lett. **108**, 032501 (2012).
[11] G. Neyens, Phys. Rev. C **84**, 064310 (2011).
[12] G. Neyens, M. Kowalska, D. Yordanov, K. Blaum, P. Himpe, P. Lievens, S. Mallion, R. Neugart, N. Vermeulen, Y. Utsuno, and T. Otsuka, Phys. Rev. Lett. **94**, 022501 (2005).
[13] M. Kimura, Phys. Rev. C **75**, 041302(R) (2007).
[14] T. Otsuka, T. Suzuki, M. Honma, Y. Utsuno, N. Tsunoda, K. Tsukiyama and M. Hjorth-Jensen, Phys. Rev. Lett. **104**, 012501 (2010).
[15] O. Niedermaier *et al.*, Phys. Rev. Lett. **94**, 172501 (2005).
[16] K. Wimmer *et al.*, Phys. Rev. Lett. **105**, 252501 (2010).
[17] J. R. Terry *et al.*, Phys. Rev. C **77**, 014316 (2008).
[18] H. T. Fortune, Phys. Rev. C **84**, 024327 (2011).

[19] G. Klotz, P. Baumann, M. Bounajma, A. Huck, A. Knipper, G. Walter, G. Marguier, C. Richard-Serre, A. Poves, and J. Retamosa, Phys. Rev. C **47**, 2502 (1993).
[20] H. Mach *et al.*, Eur. Phys. J. A **25**, s01, 105 (2005).
[21] A. M. Lane and R. G. Thomas, Rev. Mod. Phys. **30**, 257 (1958).
[22] W. J. Thompson, J. L. Adams, and D. Robson, Phys. Rev. **173**, 975 (1968).
[23] N. Imai *et al.*, Phys. Rev. C **85**, 034313 (2012).
[24] P. M. Endt, Nucl. Phys. A **633**, 1 (1998).
[25] J. Jänecke, *in Isospin in Nuclear Physics*, edited by D. H. Wilkinson (North-Holland, Amsterdam, 1969), p. 341, Eq. (8.107).
[26] E. Kugler, Hyperfine Interact. **129**, 23 (2000).
[27] V. N. Fedoseyev, G. Huber, U. Köster, J. Lettry, V. I. Mishin, H. Ravn, and V. Sebastian, Hyperfine Interact. **127**, 409 (2000).
[28] O. Kester *et al.*, Nucl. Instrum. Methods Phys. Res., Sect. B **204**, 20 (2003).
[29] J. Ziegler, SRIM-2011, http://www.srim.org/.
[30] C. R. Westerfeldt, G. E. Mitchell, E. G. Bilpuch, and D. A. Outlaw, Nucl. Phys. A **303**, 111 (1978).
[31] MINUIT, CERN program library.
[32] F. D. Becchetti, Jr. and G. W. Greenless, Phys. Rev. **182**, 1190 (1969).
[33] P. D. Kunz, University of Colorado (unpublished).
[34] S. Sen, W. A. Yoh, and M. T. McEllistrem, Phys. Rev. C **10**, 1050 (1974).
[35] R. Abegg and S. K. Datta, Nucl. Phys. A **287**, 94 (1977).
[36] M. Kimura (private communication).
[37] Y. Utsuno (private communication).
[38] B. A. Brown and W. A. Richter, Phys. Rev. C **74**, 034315 (2006).
[39] B. A. Brown and W. D. M. Rae, MSU-NSCL Report No. XX, 2007 (unpublished).